JOURNAL OF GUIDANCE, CONTROL, AND DYNAMICS
Vol. 30, No. 4, July–August 2007

Total Energy Control System for Helicopter Flight/Propulsion Integrated Controller Design

Sheng-Wen Chen*
National Cheng Kung University, Tainan City 701, Taiwan, Republic of China
Pang-Chia Chen†
Kao Yuan University, Kaohsiung County 821, Taiwan, Republic of China
Ciann-Dong Yang‡
National Cheng Kung University, Tainan City 701, Taiwan, Republic of China
and
Yaug-Fea Jeng§
Chienkuo Technology University, Changhua City 500, Taiwan, Republic of China

DOI: 10.2514/1.26670

The purpose of this paper is to design a helicopter flight control system using a total energy control system approach. A total energy control system design uses change rates of the sum and of the difference between kinetic and potential energies as control indices. This paper documents the first known application of a total energy control system design for helicopter control. Energy change rate and energy distribution rate are manipulated to provide automatic tracking of desired altitude, velocity, and flight-path-angle profiles for a Westland Lynx helicopter. A linearized helicopter dynamic model is obtained in the total energy control system framework, and control laws are synthesized using H_∞ control theory and the method of linear matrix inequalities. Numerical simulation is used to verify the effectiveness of the proposed total energy control system helicopter flight control laws. The total energy control system reduces engine fuel consumption by alleviating unnecessary fluctuations in energy change and distribution rates when tracking flight path and propulsion commands.

Nomenclature

$\dot{E}$	=	change rate of the sum of kinetic energy and potential energy
$\dot{L}$	=	change rate of the difference between the kinetic energy and potential energy
g	=	acceleration due to gravity
H, h	=	altitude and altitude perturbation, respectively
I_{xx}, I_{xz}, I_{yy}, I_{zz}	=	moment of inertia of the helicopter
L, M, N	=	aerodynamic moments about the center of gravity (body-axis coordinate system)
L_F, M_F, N_F	=	fuselage aerodynamic moments about the center of gravity (body-axis coordinate system)
L_{fn}, M_{fn}, N_{fn}	=	fin aerodynamic moments about the center of gravity (body-axis coordinate system)
L_R, M_R, N_R	=	main rotor aerodynamic moments about the center of gravity (body-axis coordinate system)
L_T, M_T, N_T	=	tail rotor moments about the center of gravity (body-axis coordinate system)
L_{tp}, M_{tp}, N_{tp}	=	tail plane aerodynamic moments about the center of gravity (body-axis coordinate system)
m	=	mass of the helicopter
p, q, r	=	fuselage coordination system x, y, z-axis angular velocity components
Q_e	=	engine torque
T_c	=	throttle valve command
u, v, w	=	fuselage coordination system x, y, z-axis velocity components
V_T, v_T	=	total velocity and total velocity deviation, respectively
X, Y, Z	=	external aerodynamic forces acting along the x, y, z axes (body-axis coordinate system)
X_F, Y_F, Z_F	=	components of X, Y, Z from the fuselage (body-axis coordinate system)
X_{fn}, Y_{fn}, Z_{fn}	=	components of X, Y, Z from the fin (body-axis coordinate system)
X_R, Y_R, Z_R	=	components of X, Y, Z from the main rotor (body-axis coordinate system)
X_T, Y_T, Z_T	=	components of X, Y, Z from the tail rotor (body-axis coordinate system)
X_{tp}, Y_{tp}, Z_{tp}	=	components of X, Y, Z from the tail plane (body-axis coordinate system)
β_0, β_{1c}, β_{1s}	=	rotor blade coning, longitudinal and lateral flapping angles
γ	=	flight path angle
θ_c	=	elevator angle command
θ_0	=	main rotor collective pitch
θ_{0T}	=	tail rotor collective pitch
θ_{1c}	=	lateral cyclic pitch
θ_{1s}	=	longitudinal cyclic pitch
φ, θ, ψ	=	Euler angles (fuselage attitude angles)
Ω	=	main rotor speed

Received 20 July 2006; revision received 18 January 2007; accepted for publication 25 January 2007.

*Graduate Student, Department of Aeronautics and Astronautics, 1 Ta-Hsueh Road.
†Associate Professor, Department of Electrical Engineering, 1821 Chung-Shan Road, Lu-Chu Hsiang. Member AIAA.
‡Professor, Department of Aeronautics and Astronautics, 1 Ta-Hsueh Road; cdyang@mail.ncku.edu.tw (Corresponding Author).
§Associate Professor, Department of Automation Engineering, 1 Chieh-Shou North Road.

I. Introduction

IN CONVENTIONAL flight control design, the autopilot system and the autothrottle system were usually considered separately: the autothrottle unit was mainly used to adjust the engine throttle valve to achieve desired flight speed, and the autopilot unit was

designed to regulate the control surfaces for altitude maneuver. However, interaction between autopilot and autothrottle systems actually exists due to the dynamic coupling between speed and altitude. The separate design approach of the two control modes leads to the drawback that controlling objectives for one control mode will disturb the objectives for another control mode. For example, if the autopilot command exceeds the drivable propulsion limit of the engine output, then the resulting speed will deviate from the autothrottle set point. The resulting unnecessary maneuver of the aircraft will increase engine fuel consumption and even cause stall or overspeed. To prevent these circumstances, many integrated flight and propulsion control designs [1,2] were proposed. A total energy control system (TECS), as one of the integrated flight and propulsion control approaches, is based on the transfer between the kinetic energy and potential energy, in which the change rates of the sum and of the difference between the kinetic energy and potential energy are used as control indices. The core idea of a TECS design is to achieve required altitude and speed by using throttle valve to control the sum of energies and by using elevator angle to control the distribution between the kinetic energy and potential energies.

As shown in Fig. 1, the integrated flight and propulsion control system for fixed-wing aircraft in the framework of a TECS provides coordination between the throttle valve command and the elevator angle command such that the undesired dynamic coupling can be effectively reduced. In addition, the mechanism of a TECS has found applications in guidance [3–5] and control [6–12] for various types of fixed-wing aircraft. Lambregts [6,7] first gave the theoretic study and set up the structure of the TECS. Warren [8] proposed that the transferring of the cruise states could be accomplished in two ways: One is by using the control laws of the *energy hold/altitude hold* to manage the propulsion and vertical lift force to maintain the required altitude and energy at a certain cruise point. The other way is via the control law of *energy obtaining*, in which the flight path angle is used to coordinate the transfer of altitude and speed to arrive at the equilibrium point. Voth and Lyt [9] employed a constrained parameter optimization approach for the tradeoffs between multiple design objectives and constraints under the TECS framework. Falerio and Lambregts [10] designed a proportional–integral feedback control law by using eigenstructure assignment based on the existing TECS structure for a linear model of the longitudinal dynamics of an aerospace technologies demonstrator (ATD) plane. It was shown that the improvement on the decoupling of the airplane flight/propulsion outputs could be achieved. Griseold [11] proposed a similar total heading control system (THCS) instead of the standard TECS design for longitudinal flight control. The dynamic coupling between the flight path angle and velocity was investigated by Ganguli and Balas [12] with an H_∞ control approach.

Though the TECS approach was developed for years for controlling fixed-wing aircraft [6–12], no previous work on the application of TECS to helicopter flight control is found. Because the coupling effects between the longitudinal and lateral dynamics of the helicopter are prominent, we need to consider the integrated longitudinal and lateral dynamics [13,14] in the helicopter TECS design, instead of simply considering the longitudinal dynamics as in the design for a fixed-wing aircraft.

Upon deriving the TECS-based output-feedback helicopter control, the various design specifications are addressed in terms of H_∞ criteria to achieve performance merits such as robustness against modelling uncertainty, bandwidth shaping of actuator output, and high fidelity of command tracking. The known literatures regarding the H_∞ technique for helicopter control include the designs for the UH-60A Black Hawk model [15] and the Yamaha R-50 robotic helicopter [16]. In this paper, the TECS-based helicopter controller satisfying the given design specification is then constructed by using the linear matrix inequality (LMI) method, which possesses the merit of numerical reliability and is especially suitable for a multiobjective controller design [17–21]. The resulting TECS design can achieve satisfactory tracking performance for the given trajectory commands by alleviating the unnecessary fluctuation of the energy change rate $\dot{E}$ and energy distribution rate $\dot{L}$ in such a way that the energy consumption for an engine can be reduced effectively.

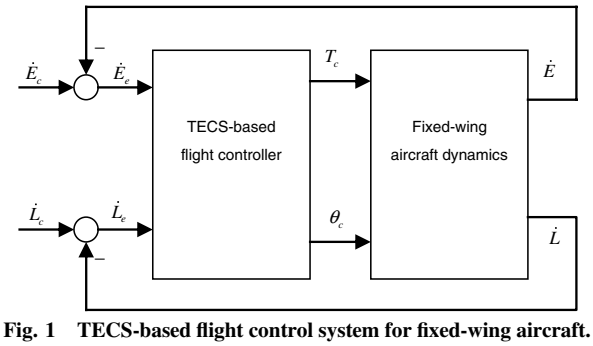

Fig. 1 TECS-based flight control system for fixed-wing aircraft.

The remainder of this paper is organized as follows. Section II introduces the derivation of the nonlinear and linearized model for the helicopter dynamics. Section III describes the theoretical aspect of a TECS and investigates its application to helicopter flight control. Section IV derives the output-feedback controller design based on H_∞ control theory and exploits the LMI method to construct the controller. Section V validates the derived TECS controller by the time-response simulations, and finally, Sec. VI gives the conclusion and future perspective.

II. Linearized Helicopter Model

For the purpose of controller design, we need to derive a suitable linearized dynamic model of the helicopter. The helicopter consists of a couple of interacting subsystems. For each of the subsystems, the states that describe its dynamic behavior are as follows:

1) For the main rotor, β_0, β_{1c}, and β_{1s} denote rotor blade coning and longitudinal and lateral flapping angles.

2) For the fuselage, u, v, w, p, q, r, ψ, θ, and ϕ denote velocities, angular velocities, and Euler angles.

3) For the engine, Ω and Q_e denote the main rotor speed and engine torque.

4) For the inflow, λ_0 and λ_{0T} denote inflows of the main rotor and tail rotor.

5) For control, θ_0, θ_{1s}, θ_{1c}, and θ_{0T} denote main rotor collective pitch, longitudinal cyclic pitch, lateral cyclic pitch, and tail rotor collective pitch.

The dynamic model of a helicopter describes a six-degree-of-freedom rigid-body motion, including the following dynamics:

For force equations,

$$\dot{u} = rv - qw + \frac{X}{M_a} - g\sin\theta \tag{1a}$$

$$\dot{v} = pw - ru + \frac{Y}{M_a} + g\sin\phi\cos\theta \tag{1b}$$

$$\dot{w} = qu - pv + \frac{Z}{M_a} + g\cos\phi\cos\theta \tag{1c}$$

for moment equations,

$$\dot{p} = (c_1 r + c_2 p)q + c_3 L + c_4 N \tag{2a}$$

$$\dot{q} = c_5 pr - c_6(p^2 - r^2) + c_7 M \tag{2b}$$

$$\dot{r} = (c_8 p - c_2 r)q + c_4 L + c_9 N \tag{2c}$$

and for attitude equations,

$$\dot{\phi} = p + \tan\theta(q\sin\phi + r\cos\phi) \tag{3a}$$

$$\dot{\theta} = q\cos\phi - r\sin\phi \tag{3b}$$

$$\dot{\psi} = (q \sin\phi + r \cos\phi)/\cos\theta \tag{3c}$$

The coefficients in the moment equations are defined as follows:

$$c_1 = [(I_{yy} - I_{zz})I_{zz} - I_{xz}^2]/\Gamma, \qquad c_2 = (I_{xx} - I_{yy} + I_{zz})I_{xz}/\Gamma, \qquad c_3 = I_{zz}/\Gamma, \qquad c_4 = I_{xz}/\Gamma, \qquad c_5 = (I_{zz} - I_{xx})/I_{yy}, \qquad c_6 = I_{xz}/I_{yy}$$
$$c_7 = 1/I_{yy}, \qquad c_8 = [(I_{xx} - I_{yy})I_{xx} + I_{xz}^2]/\Gamma, \qquad c_9 = I_{xx}/\Gamma, \qquad \Gamma = I_{xx}I_{zz} - I_{xz}^2 \tag{4}$$

The aerodynamic forces X, Y, and Z and aerodynamic moments L, M, and N are composed of contributions from the five individual subsystems and are represented as follows:

$$X = X_R + X_T + X_F + X_{\text{tp}} + X_{\text{fn}} \tag{5a}$$

$$Y = Y_R + Y_T + Y_F + Y_{\text{tp}} + Y_{\text{fn}} \tag{5b}$$

$$Z = Z_R + Z_T + Z_F + Z_{\text{tp}} + Z_{\text{fn}} \tag{5c}$$

$$L = L_R + L_T + L_F + L_{\text{tp}} + L_{\text{fn}} \tag{5d}$$

$$M = M_R + M_T + M_F + M_{\text{tp}} + M_{\text{fn}} \tag{5e}$$

$$N = N_R + N_T + N_F + N_{\text{tp}} + N_{\text{fn}} \tag{5f}$$

where the subscript R denotes the main rotor, T is the tail rotor; F is the fuselage; tp is the horizontal tail plane, and fn is the vertical fin. By the dynamic analysis for each subsystem [13], we can derive the expressions for every component in Eqs. (5), which are then substituted into Eqs. (1–3) to obtain the nonlinear dynamic equations of motion for the helicopter. The subsequent linearization about a specific flight condition yields

$$\dot{\mathbf{x}} = \mathbf{A}\mathbf{x} + \mathbf{B}\mathbf{u} \tag{6}$$

where $\mathbf{x} = [\,u \quad v \quad w \quad p \quad q \quad r \quad \phi \quad \theta\,]^T$ is the state vector, $\mathbf{u} = [\,\theta_0 \quad \theta_{1s} \quad \theta_{1c} \quad \theta_{0T}\,]^T$ is the control vector, $\mathbf{A}$ is the system matrix formed by the stability derivatives, and $\mathbf{B}$ is the input matrix formed by the control derivatives.

In this paper, the configuration data of the Westland Lynx helicopter are used to generate the numerical values of the matrices $\mathbf{A}$ and $\mathbf{B}$. At the forward velocity $u = 50$ m/s, the equilibrium trim condition is computed iteratively, as follows:

$$\begin{aligned}&[\,u \quad v \quad w \quad p \quad q \quad r \quad \phi \quad \theta \quad \Omega \quad Q_e \quad \theta_0 \quad \theta_{1s} \quad \theta_{1c} \quad \theta_{0T}\,]\\ &= [\,49.99 \quad 0 \quad -0.65 \quad 0 \quad 0 \quad 0 \quad -1.57\,\text{deg} \quad -0.74\,\text{deg} \quad 34.80 \quad 12,878 \quad 12.78\,\text{deg} \quad -2.40\,\text{deg} \quad 0.75\,\text{deg} \quad 2.77\,\text{deg}\,]\end{aligned} \tag{7}$$

At the specified trim condition, we can compute the aerodynamic forces, aerodynamic moments, and their derivatives to determine the elements of the matrices $\mathbf{A}$ and $\mathbf{B}$ as

$$\mathbf{A} = \begin{bmatrix} -0.0352 & 0.0012 & 0.0325 & -0.2392 & 1.1701 & 0 & 0 & -9.8092 \\ 0.0047 & -0.0817 & -0.0175 & -1.2591 & -0.2223 & -49.4850 & 9.8055 & -0.0035 \\ -0.0068 & -0.0099 & -0.7845 & -0.5728 & 49.8289 & -0.0002 & 0.2689 & 0.1269 \\ 0.0013 & -0.1742 & 0.0437 & -10.4135 & -2.4099 & -0.0616 & 0 & 0 \\ 0.0224 & 0.0015 & -0.0341 & 0.4800 & -2.4287 & 0.0008 & 0 & 0 \\ -0.0199 & 0.1495 & -0.0208 & -1.7324 & -0.1674 & -1.3769 & 0 & 0 \\ 0 & 0 & 0 & 1.0000 & 0.0004 & -0.0129 & 0 & 0 \\ 0 & 0 & 0 & 0 & 0.99946 & 0.0274 & 0 & 0 \end{bmatrix} \tag{8a}$$

$$\mathbf{B} = \begin{bmatrix} 0.8543 & -8.5308 & 1.5321 & 0 \\ -1.5340 & -1.8096 & -10.1354 & 6.2898 \\ -121.0973 & -38.4154 & 0.1071 & 0 \\ 11.8998 & -25.6649 & -155.2281 & -1.4233 \\ 13.7750 & 28.6663 & -5.2602 & -0.0574 \\ 11.1379 & -6.2144 & -26.9896 & -17.2164 \\ 0 & 0 & 0 & 0 \\ 0 & 0 & 0 & 0 \end{bmatrix} \tag{8b}$$

It should be noted that in this paper, the rotor angular velocity Ω and the torque Q_e are kept in their trim values, as listed in Eq. (7); no attempt was made to control Ω and Q_e. The extension of the present work to include Ω and Q_e as controlled variables, however, is a more realistic approach to integrated flight/propulsion control, which will be investigated in future research.

III. Helicopter Flight Control in the TECS Framework

In the preceding section, we derived the linearized model of the helicopter dynamics, as shown in Eqs. (8a) and (8b). In this section, the necessary modification of this dynamic equation to cope with the TECS framework will be addressed. The helicopter energy states to be controlled in TECS are defined as the sum E_T and difference L_T of the kinetic energy $(1/2)mV_T^2$ and the potential energy mgH per unit weight, that is,

$$E_T = \frac{1}{mg}\left(\frac{1}{2}mV_T^2 + mgH\right) = \frac{V_T^2}{2g} + H, \qquad L_T = \frac{1}{mg}\left(\frac{1}{2}mV_T^2 - mgH\right) = \frac{V_T^2}{2g} - H \tag{9}$$

By taking time derivatives, we then have

$$\dot{E} := \frac{\dot{E}_T}{V_T} = \frac{\dot{V}_T}{g} + \frac{\dot{H}}{V_T} = \frac{\dot{V}_T}{g} + \gamma, \qquad \dot{L} := \frac{\dot{L}_T}{V_T} = \frac{\dot{V}_T}{g} - \frac{\dot{H}}{V_T} = \frac{\dot{V}_T}{g} - \gamma \tag{10}$$

where $\gamma = \dot{H}/V_T$ is the flight path angle. The next step is to express $\dot{E}$ and $\dot{L}$ (or equivalently, $\dot{V}_T$ and $\dot{H}$) in terms of the state variables defined in Eq. (7). Assuming small perturbation with respect to the trim condition and starting with the relations $h = -(\cos\Theta_0)z + Z_0(\sin\Theta_0)\theta$ and $V_T = V_{T_0} + v_T$ with $v_T = (U_0/V_{T_0})u + (W_0/V_{T_0})w$, we can obtain the following expressions:

$$\dot{h} = (U_0\cos^2\Theta_0 + W_0\sin\Theta_0\cos\Theta_0)\theta - (\cos^2\Theta_0)w + (\cos\Theta_0\sin\Theta_0)u \tag{11}$$

$$\dot{V}_T = \dot{V}_{T0} + \dot{v}_T = \dot{v}_T = \frac{U_0}{V_{T0}}\dot{u} + \frac{W_0}{V_{T0}}\dot{w} \tag{12}$$

In the preceding expressions, we used the convention that capital letters with subscript 0 represent trim values and lowercase letters represent perturbations. By appending the preceding TECS-related variables into the state equations, as mentioned in Eqs. (8), we obtain the following augmented linearized model:

$$\begin{bmatrix} \dot{u} \\ \dot{v} \\ \dot{w} \\ \dot{p} \\ \dot{q} \\ \dot{r} \\ \dot{\phi} \\ \dot{\theta} \\ \dot{z} \end{bmatrix} = \begin{bmatrix} -0.0352 & 0.0012 & 0.0325 & -0.2392 & 1.1701 & 0 & 0 & -9.8092 & 0 \\ 0.0047 & -0.0817 & -0.0175 & -1.2591 & -0.2234 & -49.4850 & 9.8055 & -0.0035 & 0 \\ -0.0068 & -0.0099 & -0.7845 & -0.5728 & 49.8289 & -0.0002 & 0.2689 & 0.1269 & 0 \\ 0.0013 & -0.1742 & 0.0437 & -10.4135 & -2.4099 & -0.0616 & 0 & 0 & 0 \\ 0.0224 & 0.0015 & -0.0341 & 0.4800 & -2.4287 & 0.0008 & 0 & 0 & 0 \\ -0.0199 & 0.1495 & -0.0208 & -1.7324 & -0.1674 & -1.3769 & 0 & 0 & 0 \\ 0 & 0 & 0 & 1.0000 & 0.0002 & -0.0129 & 0 & 0 & 0 \\ 0 & 0 & 0 & 0 & 0.9996 & 0.0274 & 0 & 0 & 0 \\ 0.0129 & 0 & 0.9999 & 0 & 0 & 0 & 0 & -50 & 0 \end{bmatrix} \begin{bmatrix} u \\ v \\ w \\ p \\ q \\ r \\ \phi \\ \theta \\ z \end{bmatrix}$$
$$+ \begin{bmatrix} 0.8543 & -8.5348 & 1.5321 & 0 \\ -1.5430 & -1.8096 & -10.1354 & 6.2898 \\ -121.0973 & -38.4154 & 0.1071 & 0 \\ 11.8998 & -25.6649 & -155.2281 & -1.4233 \\ 13.7750 & 28.6663 & -5.2602 & -0.0574 \\ 11.1379 & -6.2144 & -26.9896 & -17.2164 \\ 0 & 0 & 0 & 0 \\ 0 & 0 & 0 & 0 \\ 0 & 0 & 0 & 0 \end{bmatrix} \begin{bmatrix} \theta_0 \\ \theta_{1s} \\ \theta_{1c} \\ \theta_{0T} \end{bmatrix} \tag{13a}$$

$$\begin{bmatrix} \dot{E} \\ \dot{L} \\ v_T \\ h \end{bmatrix} = \begin{bmatrix} -0.0038 & 0.0001 & -0.0156 & -0.0236 & 0.0536 & 0 & -0.0004 & -0.0011 & 0 \\ -0.0033 & 0.0001 & 0.0244 & -0.0236 & 0.0536 & 0 & -0.0004 & -2.0009 & 0 \\ 0.9999 & 0 & -0.0129 & 0 & 0 & 0 & 0 & 0 & 0 \\ 0 & 0 & 0 & 0 & 0 & 0 & 0 & 0 & -0.9999 \end{bmatrix} \begin{bmatrix} u \\ v \\ w \\ p \\ q \\ r \\ \phi \\ \theta \\ z \end{bmatrix}$$
$$+ \begin{bmatrix} 0.2471 & -0.8201 & 0.1562 & 0 \\ 0.2471 & -0.8201 & 0.1562 & 0 \\ 0 & 0 & 0 & 0 \\ 0 & 0 & 0 & 0 \end{bmatrix} \begin{bmatrix} \theta_0 \\ \theta_{1s} \\ \theta_{1c} \\ \theta_{0T} \end{bmatrix} \tag{13b}$$

which is denoted by the abbreviation as

$$G: \begin{cases} \dot{\mathbf{x}}_g = \mathbf{A}_g\mathbf{x}_g + \mathbf{B}_g\mathbf{u} \\ \mathbf{y}_g = \mathbf{C}_g\mathbf{x}_g + \mathbf{D}_g\mathbf{u} \end{cases} \tag{14}$$

where $\mathbf{y}_g = [\dot{E} \quad \dot{L} \quad v_T \quad h]^T$ is the augmented output measurement. As for the control input $\mathbf{u}$ for the helicopter, propulsion is controlled by the

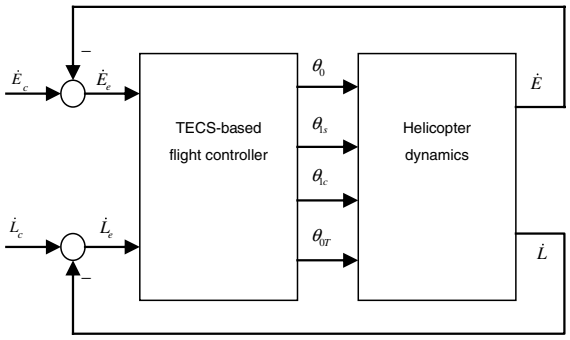

Fig. 2 TECS-based flight control system for a helicopter.

main rotor collective pitch, and attitude is adjusted by the cyclic pitches. The overall control input of the helicopter is $\mathbf{u} = (\theta_0, \theta_{1s}, \theta_{1c}, \theta_{0T})^T$, with the tail rotor collective pitch used to produce a counteracting torque of the main rotor.

The closed-loop control structure of the TECS design is illustrated in Fig. 2. Because the helicopter maneuver is based on the transfer between the kinetic energy and potential energy under the TECS framework, the objective of this control system design is to make the output response $(\dot{E}, \dot{L})^T$ track the command input $(\dot{E}_c, \dot{L}_c)^T$, which, according to Eq. (10), can be written as

$$\dot{E}_c = \frac{\dot{v}_{T_c}}{g} + \gamma_c, \qquad \dot{L}_c = \frac{\dot{v}_{T_c}}{g} - \gamma_c \tag{15}$$

IV. Output-Feedback Flight Controller Design Using the LMI Method

Referring to Fig. 2, the commands of the energy change rate $\dot{E}_c$ and the energy distribution rate $\dot{L}_c$ are considered as the external inputs to the controlled system. In Fig. 3, an internal control loop is designed for tracking the energy variables $\dot{E}$ and $\dot{L}$. Letting $\mathbf{r} = [\dot{E}_c \quad \dot{L}_c]^T$ and $\hat{\mathbf{y}} = [\dot{E} \quad \dot{L}]^T$, the input signal to the controller, denoted by $\tilde{\mathbf{y}}$, can be expressed by

$$\tilde{\mathbf{y}} = \begin{bmatrix} \dot{E}_e \\ \dot{L}_e \\ v_T \\ h \end{bmatrix} = \begin{bmatrix} \dot{E}_c - \dot{E} \\ \dot{L}_c - \dot{L} \\ v_T \\ h \end{bmatrix} = \begin{bmatrix} \mathbf{r} - \hat{\mathbf{y}} \\ v_T \\ h \end{bmatrix} \mathbf{D}_{\text{yr}}\mathbf{r} + \mathbf{D}_{\text{pr}}\mathbf{C}_g\mathbf{x}_g + \mathbf{D}_{\text{pr}}\mathbf{D}_g\mathbf{u} \tag{16}$$

with the coefficient matrices given by

$$\mathbf{D}_{\text{yr}} = \begin{bmatrix} 1 & 0 \\ 0 & 1 \\ 0 & 0 \\ 0 & 0 \end{bmatrix}, \qquad \mathbf{D}_{\text{pr}} = \begin{bmatrix} -1 & 0 & 0 & 0 \\ 0 & -1 & 0 & 0 \\ 0 & 0 & 1 & 0 \\ 0 & 0 & 0 & 1 \end{bmatrix} \tag{17}$$

Figure 4 details the mechanism generating the energy command $(\dot{E}_c, \dot{L}_c)^T$ from the altitude command $h_c(t)$ and velocity command $v_{\text{Tc}}(t)$. The altitude deviation command $h_c(t)$ is compared with the actual altitude to obtain the difference signal $h_c(t) - h(t)$ and then normalized by the parameter k_h to produce the vertical velocity

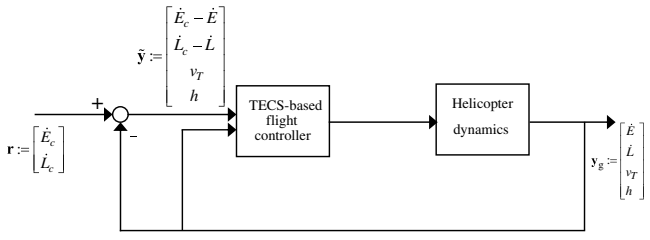

Fig. 3 Inner-loop controlled system of the TECS-based output-feedback flight controller.

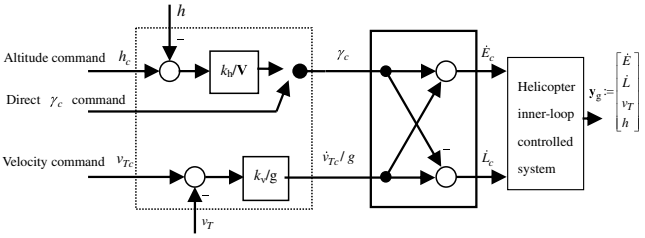

Fig. 4 Guidance commands in the outer-loop of the TECS design. There are two input channels for the γ_c command. One channel is via the altitude feedback loop and the other channel provides a feedforward path for direct γ_c command.

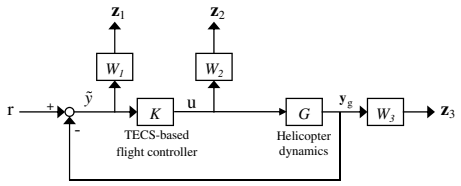

Fig. 5 Augmented control system including the weighting functions.

command $\dot{h}_c(t)$, which is further divided by the velocity v_T to give the flight-path-angle command $\gamma_c(t)$. In addition to the preceding altitude feedback loop, a direct flight-path-angle command $\gamma_c(t)$ can also be applied to form a feedforward loop of altitude control, as shown in Fig. 4. On the other hand, the command of $\dot{v}_{\text{Tc}}(t)/g$ is produced by normalizing the velocity difference $v_{Tc}(t) - v_T(t)$ with the parameter k_v/g.

The synthesis of the TECS flight controller from the input signal $\tilde{\mathbf{y}}$ is based on the H_∞ control theory to satisfy the desired robustness performance. Some appropriately chosen weighting functions are used to address the desired robustness and performance specifications, as shown in Fig. 5. The selection of the weighting function W_3 is related to the boundary of system perturbations, expressed in the form of maximum multiplicative uncertainties that can be stabilized by the same controller. Let $P_{50}(s)$ denote the nominal plant derived in Eqs. (8) with a forward speed of 50 m/s and let $P_i(s)$ denote a deviated plant. The system multiplicative uncertainty ΔP is defined as $P_i(s) - P_{50}(s) = P_{50}(s)\Delta P$, and the weighting function W_3 is employed to envelop $P_i - P_{50}$, such that

$$\bar{\sigma}(P_i - P_{50}) = \bar{\sigma}(P_{50}(s)\Delta P) \le \bar{\sigma}(P_{50}W_3) \tag{18}$$

where $\bar{\sigma}(\cdot)$ denotes the maximum singular value. By using the linearized model $P_{50}(s)$ as the nominal plant, Fig. 6 depicts the

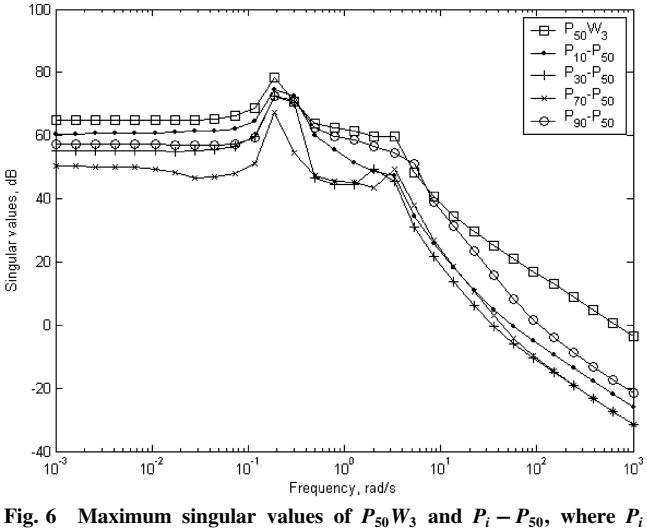

Fig. 6 Maximum singular values of $P_{50}W_3$ and $P_i - P_{50}$, where P_i denotes the perturbed plant evaluated at the four forward speeds $i = 10$, 30, 70, and 90 m/s.

boundaries of the uncertainty ΔP caused by the perturbed plants with the forward velocities 10, 30, 70, and 90 m/s, respectively. A proper weighting function W_3 with the property that the maximum singular value of $P_{50}W_3$ can cover the range of the measured uncertainties ΔP is found to be

$$W_3 = \frac{4.08(s+1)}{s+4.08} \times \mathbf{I}_{4\times 4} \tag{19}$$

The weighting function W_2 is selected to regulate control input energy. We choose W_2 as

$$W_2 = \frac{s+10}{s+100} \times \mathbf{I}_{4\times 4} \tag{20}$$

which is a high-pass filter with a cutoff frequency at 10 rad/s to limit the bandwidth of the actuator output. The growing magnitude of W_2 in the high-frequency range restrains the need of rapid response of the actuator. The choice of the weighting function W_1 affects command-tracking performance. In general, W_1 approximates a simple low-pass filter in the form of $k(1 + s/a)/s$. For the present command-tracking requirement, W_1 is chosen as

$$W_1 = \frac{0.015s + 0.45}{3s + 0.01} \times \mathbf{I}_{4\times 4} \tag{21}$$

Systematic searching methods such as Taguchi's matrix experiments and genetic algorithm were developed [14,22] to determine the preceding weighting functions to satisfy the helicopter handling-qualities specifications (ADS-33) [23].

By introducing state-space representations of the chosen weighting functions, the input–output relationship of each weighting function can be written as follows:

$$W_1: \begin{cases} \dot{\mathbf{x}}_1 = \mathbf{A}_{w1}\mathbf{x}_1 + \mathbf{B}_{w1}\mathbf{D}_{yw}\mathbf{r} + \mathbf{B}_{w1}\mathbf{D}_{pr}\mathbf{C}_g\mathbf{x}_g + \mathbf{B}_{w1}\mathbf{D}_{pr}\mathbf{D}_g\mathbf{u} \\ \mathbf{z}_1 = \mathbf{C}_{w1}\mathbf{x}_1 + \mathbf{D}_{w1}\mathbf{D}_{yw}\mathbf{r} + \mathbf{D}_{w1}\mathbf{D}_{pr}\mathbf{C}_g\mathbf{x}_g + \mathbf{D}_{w1}\mathbf{D}_{pr}\mathbf{D}_g\mathbf{u} \end{cases} \tag{22a}$$

$$W_2: \begin{cases} \dot{\mathbf{x}}_2 = \mathbf{A}_{w2}\mathbf{x}_2 + \mathbf{B}_{w2}\mathbf{u} \\ \mathbf{z}_2 = \mathbf{C}_{w2}\mathbf{x}_2 + \mathbf{D}_{w2}\mathbf{u} \end{cases} \tag{22b}$$

$$W_3: \begin{cases} \dot{\mathbf{x}}_3 = \mathbf{A}_{w3}\mathbf{x}_3 + \mathbf{B}_{w3}\mathbf{C}_g\mathbf{x}_g + \mathbf{B}_{w3}\mathbf{D}_g\mathbf{u} \\ \mathbf{z}_3 = \mathbf{C}_{w3}\mathbf{x}_3 + \mathbf{D}_{w3}\mathbf{C}_g\mathbf{x}_g + \mathbf{D}_{w3}\mathbf{D}_g\mathbf{u} \end{cases} \tag{22c}$$

The integration of the helicopter dynamics in Eq. (14) with the weighting dynamics in Eqs. (22) and the measurement $\tilde{\mathbf{y}}$ in Eq. (16) leads to the following augmented system:

$$\begin{bmatrix} \dot{\mathbf{x}}_g \\ \dot{\mathbf{x}}_1 \\ \dot{\mathbf{x}}_2 \\ \dot{\mathbf{x}}_3 \end{bmatrix} = \begin{bmatrix} \mathbf{A}_g & \mathbf{0} & \mathbf{0} & \mathbf{0} \\ \mathbf{B}_{w1}\mathbf{D}_{pr}\mathbf{C}_g & \mathbf{A}_{w1} & \mathbf{0} & \mathbf{0} \\ \mathbf{0} & \mathbf{0} & \mathbf{A}_{w2} & \mathbf{0} \\ \mathbf{B}_{w3}\mathbf{C}_g & \mathbf{0} & \mathbf{0} & \mathbf{A}_{w3} \end{bmatrix} \begin{bmatrix} \mathbf{x}_g \\ \mathbf{x}_1 \\ \mathbf{x}_2 \\ \mathbf{x}_3 \end{bmatrix} + \begin{bmatrix} \mathbf{0} \\ \mathbf{B}_{w1}\mathbf{D}_{yw} \\ \mathbf{0} \\ \mathbf{0} \end{bmatrix} \mathbf{r} + \begin{bmatrix} \mathbf{B}_g \\ \mathbf{B}_{w1}\mathbf{D}_{pr}\mathbf{D}_g \\ \mathbf{B}_{w2} \\ \mathbf{B}_{w3}\mathbf{D}_g \end{bmatrix} \mathbf{u} \tag{23a}$$

$$\begin{bmatrix} \mathbf{z}_1 \\ \mathbf{z}_2 \\ \mathbf{z}_3 \end{bmatrix} = \begin{bmatrix} \mathbf{D}_{w1}\mathbf{D}_{pr}\mathbf{C}_g & \mathbf{C}_{w1} & \mathbf{0} & \mathbf{0} \\ \mathbf{0} & \mathbf{0} & \mathbf{C}_{w2} & \mathbf{0} \\ \mathbf{D}_{w3}\mathbf{C}_g & \mathbf{0} & \mathbf{0} & \mathbf{C}_{w3} \end{bmatrix} \begin{bmatrix} \mathbf{x}_g \\ \mathbf{x}_1 \\ \mathbf{x}_2 \\ \mathbf{x}_3 \end{bmatrix} + \begin{bmatrix} \mathbf{D}_{w1}\mathbf{D}_{yw} \\ \mathbf{0} \\ \mathbf{0} \end{bmatrix} \mathbf{r} + \begin{bmatrix} \mathbf{D}_{w1}\mathbf{D}_{pr}\mathbf{D}_g \\ \mathbf{D}_{w2} \\ \mathbf{D}_{w3}\mathbf{D}_g \end{bmatrix} \mathbf{u} \tag{23b}$$

$$\mathbf{y} = \tilde{\mathbf{y}} = [\mathbf{D}_{pr}\mathbf{C}_g \quad \mathbf{0} \quad \mathbf{0} \quad \mathbf{0}] \begin{bmatrix} \mathbf{x}_g \\ \mathbf{x}_1 \\ \mathbf{x}_2 \\ \mathbf{x}_3 \end{bmatrix} + \mathbf{D}_{yr}\mathbf{r} + \mathbf{D}_{pr}\mathbf{D}_g\mathbf{u} \tag{23c}$$

which are denoted as

$$\begin{gathered} \dot{\mathbf{x}} = \mathbf{A}\mathbf{x} + \mathbf{B}_r\mathbf{r} + \mathbf{B}\mathbf{u}, \qquad \mathbf{z} = \mathbf{C}_z\mathbf{x} + \mathbf{D}_{zr}\mathbf{r} + \mathbf{D}_{zu}\mathbf{u} \\ \mathbf{y} = \mathbf{C}_y\mathbf{x} + \mathbf{D}_{yr}\mathbf{r} + \mathbf{D}_{yu}\mathbf{u} \end{gathered} \tag{24}$$

with the augmented state vector $\mathbf{x}^T := [\mathbf{x}_g^T \quad \mathbf{x}_1^T \quad \mathbf{x}_2^T \quad \mathbf{x}_3^T]$ and the penalty output $\mathbf{z}^T := [\mathbf{z}_1^T \quad \mathbf{z}_2^T \quad \mathbf{z}_3^T]$.

The control $\mathbf{u}$ to be designed has the proper type of structure:

$$\dot{\mathbf{x}}_k = \mathbf{A}_k\mathbf{x}_k + \mathbf{B}_k\mathbf{y}, \qquad \mathbf{u} = \mathbf{C}_k\mathbf{x}_k + \mathbf{D}_k\mathbf{y} \tag{25}$$

where the coefficient matrices $\mathbf{A}_k$, $\mathbf{B}_k$, $\mathbf{C}_k$, and $\mathbf{D}_k$ are to be determined by the LMI formulation. Substituting the variable $\mathbf{y}$ from Eq. (24) into the control $\mathbf{u}$ in Eq. (25), we have

$$\mathbf{u} = \bar{\mathbf{C}}_k\mathbf{x}_k + \bar{\mathbf{D}}_k\mathbf{C}_y\mathbf{x} + \bar{\mathbf{D}}_k\mathbf{D}_{yr}\mathbf{r} \tag{26}$$

where

$$\bar{\mathbf{C}}_k := (\mathbf{I} - \mathbf{D}_k\mathbf{D})^{-1}\mathbf{C}_k, \qquad \bar{\mathbf{D}}_k := (\mathbf{I} - \mathbf{D}_k\mathbf{D}_{yu})^{-1}\mathbf{D}_k \tag{27}$$

Further substitution of the preceding $\mathbf{u}$ into Eqs. (24) and (25) yields the closed-loop system:

$$\begin{cases} \dot{\mathbf{x}}_{cl} = \mathbf{A}_{cl}\mathbf{x} + \mathbf{B}_{cl}\mathbf{r} \\ \mathbf{z} = \mathbf{C}_{cl}\mathbf{x}_{cl} + \mathbf{D}_{cl}\mathbf{r}, \end{cases} \qquad \mathbf{x}_{cl} := \begin{bmatrix} \mathbf{x} \\ \mathbf{x}_k \end{bmatrix} \tag{28}$$

where the closed-loop matrices in the preceding state-space representation are obtained as

$$\begin{gathered} \mathbf{A}_{cl} := \begin{bmatrix} \mathbf{A} + \mathbf{B}\bar{\mathbf{D}}_k\mathbf{C}_y & \mathbf{B}\bar{\mathbf{C}}_k \\ \mathbf{B}_k\mathbf{C}_y + \mathbf{B}_k\mathbf{D}_{yu}\bar{\mathbf{D}}_k\mathbf{C}_y & \mathbf{A}_k + \mathbf{B}_k\mathbf{D}_{yu}\bar{\mathbf{C}}_k \end{bmatrix} \\ \mathbf{B}_{cl} := \begin{bmatrix} \mathbf{B}_r + \mathbf{B}\bar{\mathbf{D}}_k\mathbf{D}_{yrr} \\ \mathbf{B}_k\mathbf{D}_{yr} + \mathbf{B}_k\mathbf{D}_{yu}\bar{\mathbf{D}}_k\mathbf{D}_{yr} \end{bmatrix} \end{gathered} \tag{29a}$$

$$\mathbf{C}_{cl} := [\mathbf{C}_z + \mathbf{D}_{zu}\bar{\mathbf{D}}_k\mathbf{C}_y \quad \mathbf{D}_{zu}\bar{\mathbf{C}}_k], \qquad \mathbf{D}_{cl} := [\mathbf{D}_{zr} + \mathbf{D}_{zu}\bar{\mathbf{D}}_k\mathbf{D}_{yr}] \tag{29b}$$

H_∞ control theory assures robustness to system modeling uncertainty while meeting performance specifications, such as closed-loop bandwidth, that are defined in the frequency domain. The achievement of H_∞ performance for a certain closed-loop system can be addressed by the following LMI formulation. For a designated performance level $\lambda > 0$, the closed-loop system (28) is stable and satisfies the performance constraint on the transfer matrix $\|\mathrm{T}_{rz}\|_\infty < \lambda$, if and only if there exists a positive definite matrix $\mathbf{P} = \mathbf{P}^T > 0$, such that the following LMI condition holds:

$$\begin{bmatrix} \mathbf{A}_{cl}^T\mathbf{P} + \mathbf{P}\mathbf{A}_{cl} & \mathbf{P}\mathbf{B}_{cl} & \mathbf{C}_{cl}^T \\ \mathbf{B}_{cl}^T & -\lambda\mathbf{I} & \mathbf{D}_{cl}^T \\ \mathbf{C}_{cl} & \mathbf{D}_{cl} & -\lambda\mathbf{I} \end{bmatrix} < 0 \tag{30}$$

The value of $1/\lambda$ can be conceived of as a measure of gain-phase margin, and the minimum allowable λ gives an indication of the maximum achievable stability margin. Let the matrices $\mathbf{P}$ and $\mathbf{P}^{-1}$ be partitioned as

$$\mathbf{P} = \begin{bmatrix} \mathbf{Y} & \mathbf{N} \\ \mathbf{N}^T & \mathbf{V} \end{bmatrix}, \qquad \mathbf{P}^{-1} = \begin{bmatrix} \mathbf{X} & \mathbf{M} \\ \mathbf{M}^T & \mathbf{U} \end{bmatrix}$$

where the dimension of these matrix variables conforms to the state $\mathbf{x}_{cl}$ of the closed-loop system. Defining two new matrix variables

$$\boldsymbol{\varphi}_1 = \begin{bmatrix} \mathbf{X} & \mathbf{I} \\ \mathbf{M}^T & \mathbf{0} \end{bmatrix}, \qquad \boldsymbol{\varphi}_2 = \begin{bmatrix} \mathbf{I} & \mathbf{Y} \\ \mathbf{0} & \mathbf{N}^T \end{bmatrix}$$

we can verify the relationship

$$\mathbf{P}\boldsymbol{\varphi}_1 = \boldsymbol{\varphi}_2, \qquad \boldsymbol{\varphi}_1^T \mathbf{P} \boldsymbol{\varphi}_1 = \boldsymbol{\varphi}_1^T \boldsymbol{\varphi}_2 = \begin{bmatrix} \mathbf{X} & \mathbf{I} \\ \mathbf{I} & \mathbf{Y} \end{bmatrix} > \mathbf{0} \tag{31}$$

By pre- and postmultiplying the block diagonal matrices $\text{diag}(\boldsymbol{\varphi}_1^T, \mathbf{I}, \mathbf{I})$ and $\text{diag}(\boldsymbol{\varphi}_1, \mathbf{I}, \mathbf{I})$ in the matrix inequality (30), we obtain

$$\begin{bmatrix} \mathbf{J}_a^T + \mathbf{J}_a & \mathbf{J}_b & \mathbf{J}_c \\ \mathbf{J}_b^T & -\lambda \mathbf{I} & \mathbf{J}_d \\ \mathbf{J}_c^T & \mathbf{J}_d^T & -\lambda \mathbf{I} \end{bmatrix} < \mathbf{0} \tag{32}$$

wherein the matrix variables are defined as

$$\mathbf{J}_a = \begin{bmatrix} \mathbf{AX} + \mathbf{B}\mathcal{C}_\mathcal{K} & \mathbf{A} + \mathbf{B}\mathcal{D}_\mathcal{K}\mathbf{C}_y \\ \mathcal{A}_\mathcal{K} & \mathbf{YA} + \mathcal{B}_\mathcal{K}\mathbf{C}_y \end{bmatrix}$$
$$\mathbf{J}_b = \begin{bmatrix} \mathbf{B}_r + \mathbf{B}\mathcal{D}_\mathcal{K}\mathbf{D}_{\text{yr}} \\ \mathbf{YB}_r + \mathcal{B}_\mathcal{K}\mathbf{D}_{\text{yr}} \end{bmatrix} \tag{33}$$

$$\mathbf{J}_c = \begin{bmatrix} \mathbf{X}\mathbf{C}_z^T + \mathcal{C}_\mathcal{K}^T\mathbf{D}_{\text{zu}}^T \\ \mathbf{C}_z^T + \mathbf{C}_y^T\mathcal{D}_\mathcal{K}^T\mathbf{D}_{\text{zu}}^T \end{bmatrix}, \qquad \mathbf{J}_d = [\mathbf{D}_{\text{zr}}^T + \mathbf{D}_{\text{yr}}^T\mathcal{D}_\mathcal{K}^T\mathbf{D}_{\text{zu}}^T] \tag{34}$$

and the following new controller parameters are introduced:

$$\begin{gathered} \mathcal{D}_\mathcal{K} := \bar{\mathbf{D}}_k \qquad \mathcal{C}_\mathcal{K} := \mathcal{D}_\mathcal{K}\mathbf{C}_y\mathbf{X} + \bar{\mathbf{C}}_k\mathbf{M}^T \\ \mathcal{B}_\mathcal{K} := \mathbf{YB}\mathcal{D}_\mathcal{K} + \mathbf{N}\mathbf{B}_k(\mathbf{I} + \mathbf{D}_{\text{yu}}\mathcal{D}_\mathcal{K}) \\ \mathcal{A}_\mathcal{K} := \mathbf{YAX} + \mathbf{N}\mathbf{B}_k\mathbf{C}_y\mathbf{X} + \mathbf{N}\mathbf{A}_k\mathbf{M} + (\mathbf{YB} + \mathbf{N}\mathbf{B}_k\mathbf{D}_{\text{yu}})\mathcal{C}_\mathcal{K} \end{gathered} \tag{35}$$

We can find that the matrix inequality (32) is indeed an LMI condition in terms of the matrix variables $\mathbf{X}$, $\mathbf{Y}$, $\mathcal{A}_\mathcal{K}$, $\mathcal{B}_\mathcal{K}$, $\mathcal{C}_\mathcal{K}$, and $\mathcal{D}_\mathcal{K}$, which can be solved numerically by using standard LMI algorithms. For example, in the MATLAB [24] LMI Toolbox environment, we can try to find a set of feasible solutions under a given performance level λ or to find an optimal solution minimizing the performance level λ. Once the matrix variables $\mathbf{X}$, $\mathbf{Y}$, $\mathcal{A}_\mathcal{K}$, $\mathcal{B}_\mathcal{K}$, $\mathcal{C}_\mathcal{K}$, and $\mathcal{D}_\mathcal{K}$ are solved, the invertible square matrices $\mathbf{M}$ and $\mathbf{N}$ can be computed by a singular value decomposition algorithm. Then, we can solve for $\mathbf{A}_k$, $\mathbf{B}_k$, $\bar{\mathbf{C}}_k$, and $\bar{\mathbf{D}}_k$ from Eq. (35), and by Eq. (27), we can obtain the controller parameters $\mathbf{A}_k$, $\mathbf{B}_k$, $\mathbf{C}_k$, and $\mathbf{D}_k$ having the desired proper-type controller structure, as shown in Eq. (25).

V. Simulations and Discussions

The simulation is conducted in the MATLAB Simulink environment. Figures 3 and 4 display the block diagrams for the flight controller design, which are used in the following time-response simulations. Figure 3 is the internal loop of the TECS closed-loop control system. Figure 4 shows the outer-loop mechanism to provide various command signals such as the guidance velocity, altitude, and flight path angle to the internal-loop control system. In Fig. 4, the block labeled "helicopter inner-loop control system" represents the whole control system contained in Fig. 3. In this simulation, the values of the normalizing parameters k_h and k_v, as shown in Fig. 4, are chosen as $k_h = 0.5$ and $k_v = 0.5$.

The input signals to the time-response simulations are step commands of altitude deviation h_c, velocity deviation v_{Tc}, and flight path angle γ_c. Figures 7 and 8 depict the time responses to an altitude deviation command $h_c = 20$ m; Figs. 9 and 10 are time responses to a velocity deviation command $v_{Tc} = 5$ m/s, and Figs. 11 and 12 illustrate the time responses to a pulse flight-path-angle command $\gamma_c = 10$ deg with a duration of 50 s. The tracking performances of altitude, velocity, and flight path angle are manifested, respectively, in Figs. 7, 9, and 11, in which the dashed lines show the command signals of h_c, v_{Tc}, $\dot{E}_c$, $\dot{L}_c$, and γ_c, and the solid lines show their actual time responses. The corresponding blade angle control for the preceding three command inputs is shown in Figs. 8, 10, and 12, respectively.

In the time responses to an altitude deviation command $h_c = 20$ m, as shown in Figs. 7 and 8, an initially increasing main rotor collective pitch provides an increasing total energy rate $\dot{E}$ and thus accumulates a desired altitude increment. By comparing the commanded and actual energy change rate $\dot{E}$ and distribution rate $\dot{L}$ and noting that the commanded $\dot{E}_c$ and $\dot{L}_c$ exhibit more fluctuations than their actual responses $\dot{E}$ and $\dot{L}$, we can see that the introduced

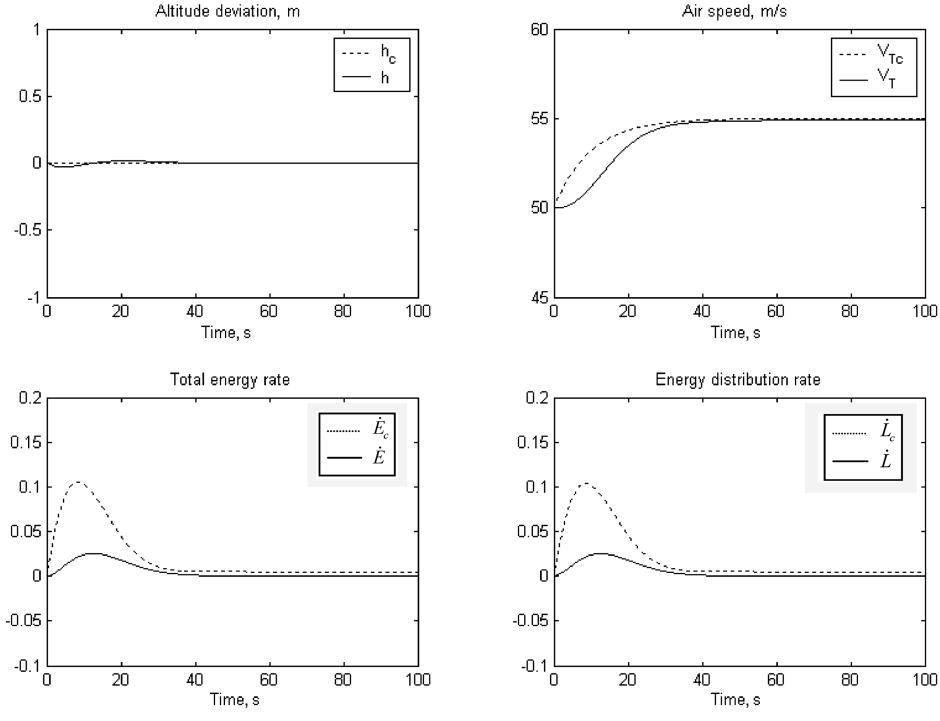

Fig. 7 Output responses to the commands $h_c = 20$ m and $v_{Tc} = 0$ m/s.

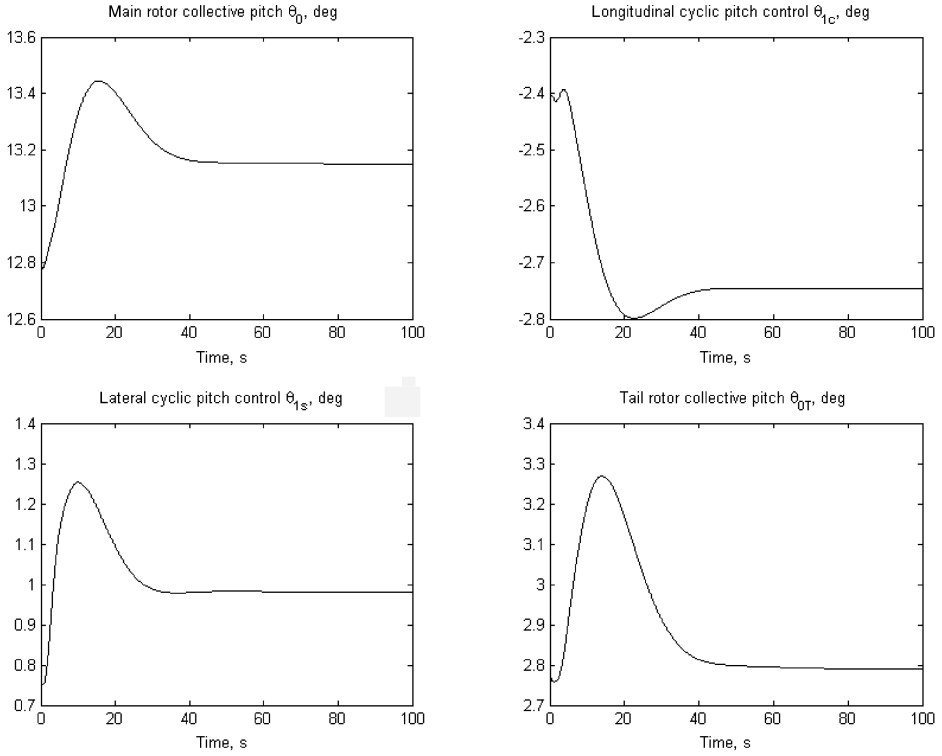

Fig. 8 Control pitch angles in response to the command $h_c = 20$ m and $v_{Tc} = 0$ m/s.

TECS control scheme does alleviate the unnecessary fluctuation of the energy change rate $\dot{E}$ and the energy distribution rate $\dot{L}$.

In Figs. 9 and 10 regarding the time responses to a velocity deviation command $v_{Tc} = 5$ m/s, the speed increment is attained by an initially decreasing longitudinal pitch control θ_{1s}, a positive lateral pitch θ_{1c}, and a tail rotor collective pitch θ_{0T} to maintain torque balance and also by a positive main rotor collective pitch θ_0 to maintain altitude. As we can see, the responses of the total energy change rate $\dot{E}$ and the energy distribution rate $\dot{L}$ are almost the same because the flight path angle is nearly zero in this case of zero altitude command. Furthermore, the introduced TECS scheme achieves a smooth tracking trajectory in such a way that the actual energy change and distribution rates exhibit less fluctuations than the commanded energy change and distribution rates. For the Westland Lynx helicopter, its admissible pitch angles are operated in the following ranges: $6.25\,\text{deg} \le \theta_0 \le 23.25\,\text{deg}$, $-8.7\,\text{deg} \le \theta_{1s} \le 14\,\text{deg}$, $-7\,\text{deg} \le \theta_{1c} \le 8\,\text{deg}$, and $-40\,\text{deg} \le \theta_{0T} \le 40\,\text{deg}$. In comparison with their full operation ranges, we can see from Fig. 10 that the oscillation of the control efforts θ_0 , θ_{1s}, θ_{1c}, and θ_{0T} in the TECS scheme is comparatively small.

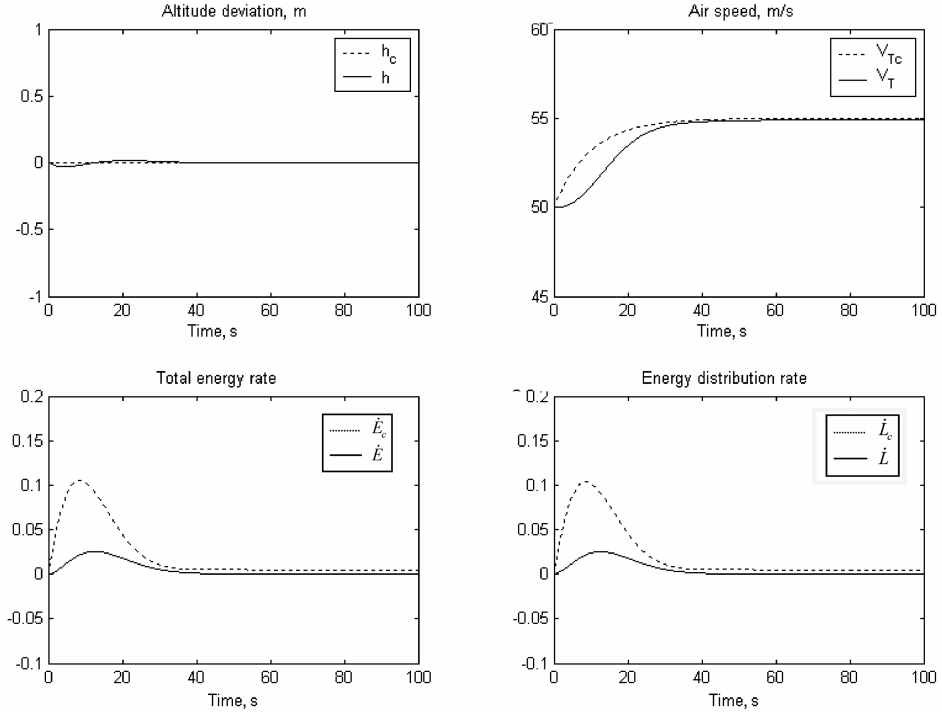

Fig. 9 Output responses to the commands $h_c = 0$ m and $v_{Tc} = 5$ m/s.

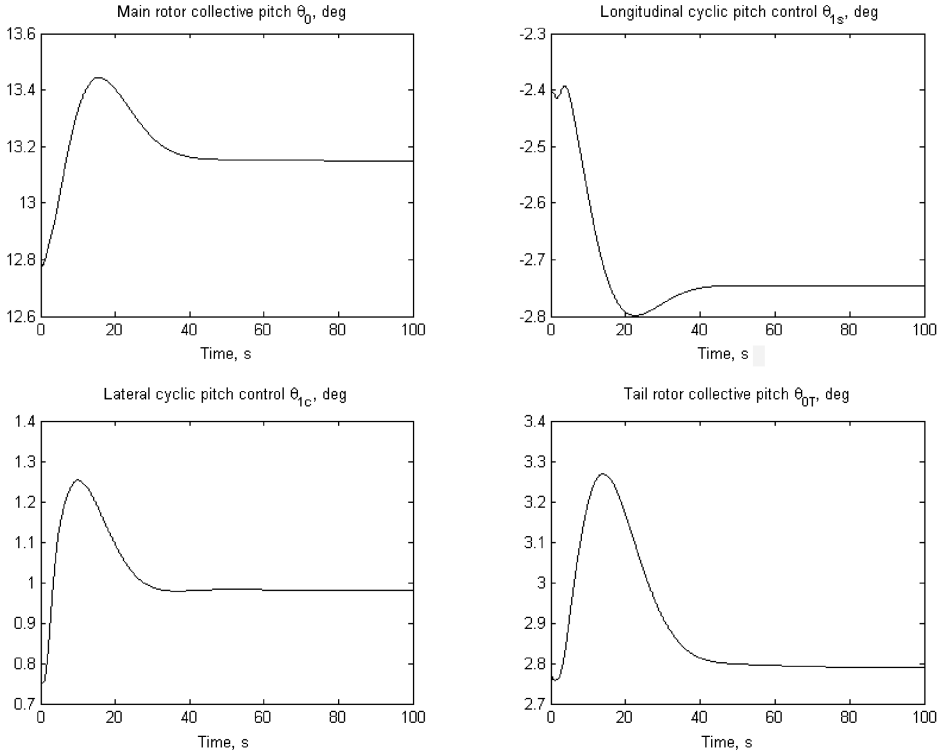

Fig. 10 Control pitch angles in response to the commands $h_c = 0$ m and $v_{Tc} = 5$ m/s.

Figures 11 show the time responses to a feedforward flight-path-angle command $\gamma_c = 10$ deg with pulse duration of 50 s. In this situation, the altitude deviation h gradually increases to reach about 435 m, as indicated by the dashed-dotted line in a unit of 100 m. The vertical speed corresponding to $\gamma_c = 10$ deg is $V_{T0}\sin(\gamma_c) = 50\sin 10\,\text{deg} = 8.68$ m/s, and the resulting altitude change in 50 s is $8.68 \times 50 = 434$ m, which provides a good estimate of the altitude increment, as observed in Fig. 11. The blade pitch angles in response to this flight-path-angle command are demonstrated in Fig. 12. It can be seen that θ_0 and θ_{0T} respond correctly to cope with the γ_c command, whereas the operation of the cyclic pitches θ_{1c} and θ_{1s} contributes to the appropriate responses of the attitude and velocity maneuvering. Meanwhile, it is noticed that the time responses of the four blade pitches all start from their trim values, as listed in Eq. (7), and return to the same trim values at the end of the γ_c command. As shown in Fig. 11, the TECS control mechanism again reduces the fluctuation of $\dot{E}$ and $\dot{L}$ in comparison with the commanded $\dot{E}_c$ and $\dot{L}_c$, and thus gives rise to smooth control efforts without unnecessary fluctuation. Consequently, control effort and engine energy were not wasted during this control mission.

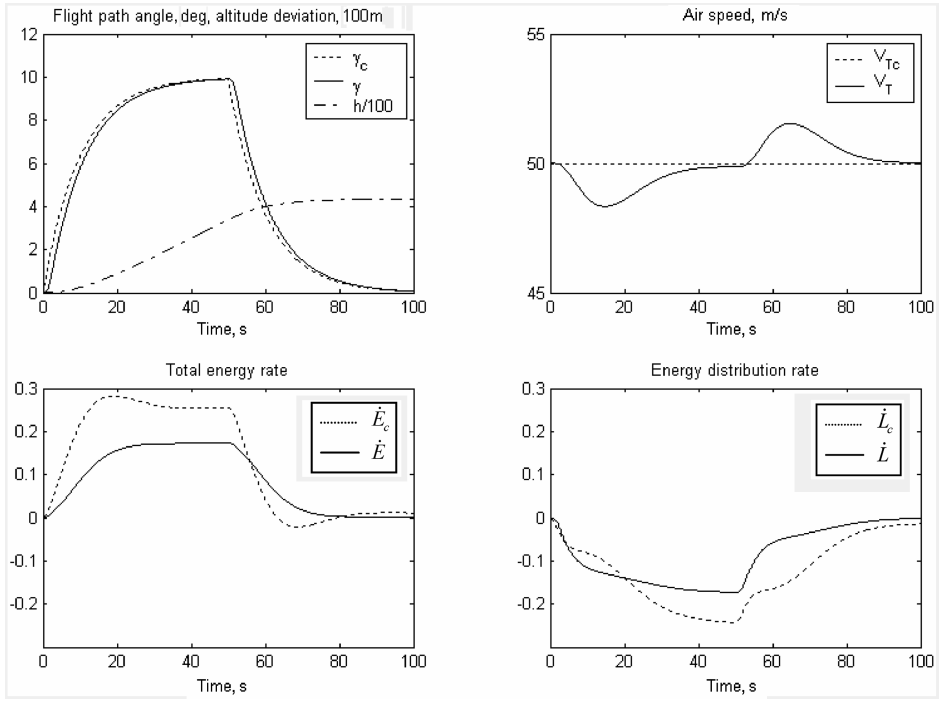

Fig. 11 Output responses to the commands $\gamma_c = 10$ deg and $v_{Tc} = 0$ m/s.

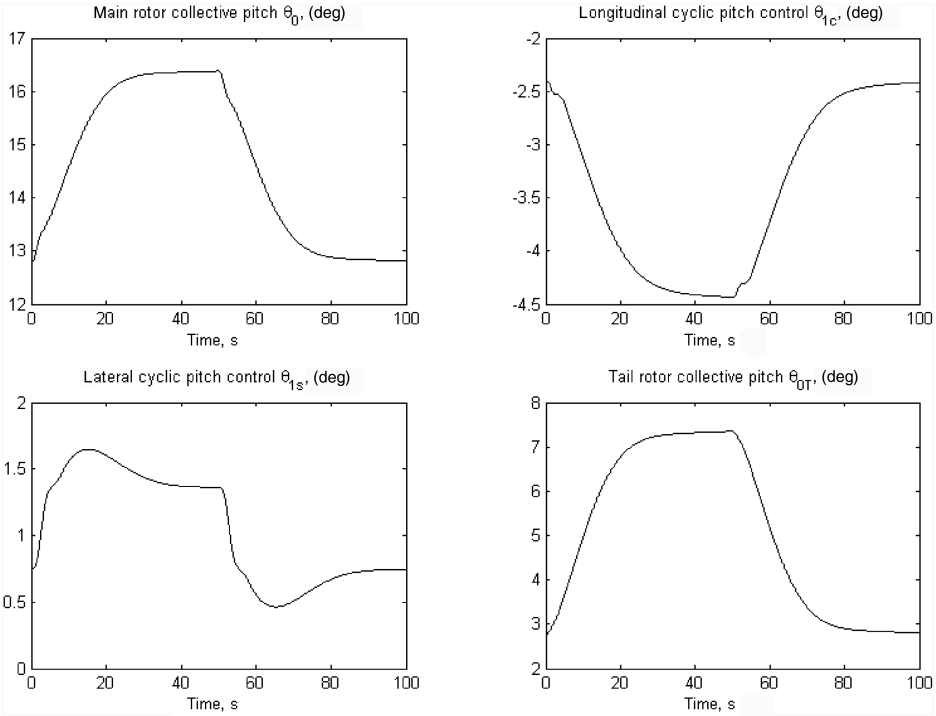

Fig. 12 Control pitch angles in response to the commands $\gamma_c = 10\,\mathrm{deg}$ and $v_{Tc} = 0\ \mathrm{m/s}$.

VI. Conclusions

This paper addressed helicopter control design using the total energy control system approach. According to the total energy command, the output-feedback flight controller with H_∞ performance was constructed by using the linear matrix inequality approach. The effectiveness of the resulting TECS design was verified in the numerical simulations, showing that a linear dynamic model of the Westland Lynx helicopter is able to achieve the expected objectives of flight stability and total energy command tracking. By using this TECS design, the pilot has a simpler operating interface; the only thing for the pilot to do is to input the desired altitude and velocity commands, or alternatively, the flight-path-angle and velocity commands, and the integrated flight/propulsion control system will perform the rest. Furthermore, under the TECS framework, not only the dynamic coupling between the velocity and altitude can be lowered, but also the magnitude constraints on the energy change rate and the energy distribution rate can be specified so that flight safety is improved and accident rates are reduced.

References

[1] Sahasrabudhe, V., Celi, R., and Tits, A. L., "Integrated Rotor-Flight Control Optimization with Aeroelastic and Handling Qualities Constraints," *Journal of Guidance, Control, and Dynamics*, Vol. 20, No. 2, 1997, pp. 217–224.

[2] Postlethwaite, I., and Bates, G., "Robust Integrated Flight and Propulsion Controller for the Harrier Aircraft," *Journal of Guidance, Control, and Dynamics*, Vol. 22, No. 2, 1994, pp. 286–290.

[3] Kaminer, I., and O'shaughnessy, P., "Integration of Four-Dimensional Guidance with Total Energy Control System," *Journal of Guidance, Control, and Dynamics*, Vol. 14, No. 3, 1991, pp. 564–573.

[4] Wu, S. F., and Guo, S. F., "Optimum Flight Trajectory Guidance Based on Total Energy Control of Aircraft," *Journal of Guidance, Control, and Dynamics*, Vol. 17, No. 2, 1994, pp. 291–296.

[5] Schmidt, D. K., and Hermann, J. A., "Use of Energy-State Analysis on a Genetic Air-Breathing Hyperbolic Vehicle," *Journal of Guidance, Control, and Dynamics*, Vol. 21, No. 1, 1998, pp. 71–76.

[6] Lambregts, A. A., "Integrated System Design for Flight and Propulsion Control Using Total Energy Principles," AIAA Paper 83-2561, 1983.

[7] Lambregts, A. A., "Vertical Flight Path and Speed Control Autopilot Design Using Total Energy Principles," AIAA Paper 83-2239, 1983.

[8] Warren, A., "Application of Total Energy Control for High-Performance Aircraft Vertical Transitions," *Journal of Guidance, Control, and Dynamics*, Vol. 14, No. 2, 1991, pp. 447–452.

[9] Voth, C., and Lyt, U. L., "Design of a Total Energy Control Autopilot Using Constrained Parameter Optimization," *Journal of Guidance, Control, and Dynamics*, Vol. 14, No. 5, 1991, pp. 927–935.

[10] Falerio, L. F., and Lambregts, A. A., "Analysis and Tuning of a Total Energy Control System Control Law Using Eigenstructure Assignment," *Aerospace Science and Technology*, Vol. 4, No. 3, 1999, pp. 127–140.

[11] Griseold, J., "Integrated Flight and Propulsion Control System Design for a Business Jet," AIAA Paper 00-4542, 2000.

[12] Ganguli, S., and Balas, G., "A TECS Alternative Using Robust Multivariable Control," AIAA Paper 01-4022, 2001.

[13] Padfield, G. O., *Helicopter Flight Dynamics: The Theory and Application of Flying Qualities and Simulation on Modeling*, AIAA, Reston, VA, 1996.

[14] Luo, C. C., Liu, R. F., Yang, C. D., and Chang, Y. H., "Helicopter H_∞ Control Design with Robust Flying Quality," *Aerospace Science and Technology*, Vol. 7, No. 2, 2003, pp. 159–169.

[15] Takahashi, M. D., "H_∞ Helicopter Flight Control Law Design with and Without Rotor State Feedback," *Journal of Guidance, Control, and Dynamics*, Vol. 17, No. 6, 1994, pp. 1245–1251.

[16] Civita, M. L., Papageorgiou, G., Messner, W. C., and Tanade, T., "Design and Flight Testing of an H_∞ Controller for a Robotic Helicopter," *Journal of Guidance, Control, and Dynamics*, Vol. 29, No. 2, 2006, pp. 485–494.

[17] Boyd, S., Ghaoui, L. E., Feron, E., and Balakrishnan, V., *Linear Matrix Inequalities in System and Control Theory*, Society for Industrial and Applied Mathematics, Philadelphia, 1994.

[18] Yang, C. D., and Sun, Y. P., "Mixed H_2/H_∞ State-Feedback Design for Microsatellite Attitude Control," *Control Engineering Practice*, Vol. 10, No. 9, 2002, pp. 951–970.

[19] Mahmoud, C., and Gahinet, P., "H_∞ Design with Placement Constraints: an LMI Approach," *IEEE Transactions on Automatic Control*, Vol. 41, No. 3, 1996, pp. 358–367.

[20] Scherer, C., Gahinet, P., and Chilali, M., "Multiobjective Output-Feedback Control via LMI Optimization," *IEEE Transactions on Automatic Control*, Vol. 42, No. 7, 1997, pp. 896–911.

[21] Zheng, F., Wang, Q. G., and Lee, T. H., "On the Design of Multivariable PID Controllers Via LMI Approach," *Automatica*, Vol. 38, No. 3, 2002, pp. 517–526.

[22] Yang, C. D., Luo, C. C., Liu, S. J., and Chang, Y. H., "Applications of Genetic-Taguchi Algorithm in Flight Control Designs," *Journal of Aerospace Engineering*, Vol. 18, No. 4, 2005, pp. 232–241.

[23] "Aeronautical Design Standard ADS-33C—Handling Qualities for Military Helicopters," U.S. Army Aviation Systems Command 1989.

[24] Gahinet, P., Nemirovski, A., Laub, A. J., and Chilali, M., *LMI Control Toolbox User's Guide*, The MathWorks, Natick, MA, 1995.